

Supplemental Material for

# Mercury evidence of Deccan volcanism driving the Latest Maastrichtian warming event

**Sha Li<sup>1</sup>, Stephen E. Grasby<sup>2</sup>, Xiangdong Zhao<sup>1</sup>, Jiubin Chen<sup>3</sup>, Daran Zheng<sup>1</sup>, He Wang<sup>1</sup>, Yanan Fang<sup>1</sup>, Qi Zhang<sup>4</sup>, Tingting Yu<sup>1</sup>, Jingxiang Tian<sup>5</sup>, Shengxian Du<sup>5</sup>, Edmund A. Jarzembowski<sup>1,6</sup>, Qifei Wang<sup>1</sup>, Haichun Zhang<sup>1</sup>, Xiaoqiao Wan<sup>7</sup>, Bo Wang<sup>1</sup>**

*<sup>1</sup>State Key Laboratory of Palaeobiology and Stratigraphy, Nanjing Institute of Geology and Palaeontology and Center for Excellence in Life and Palaeoenvironment, Chinese Academy of Sciences, Nanjing 210008, China*

*<sup>2</sup>Geological Survey of Canada, 3303 33rd Street NW, Calgary, AB T2L 2A7, Canada*

*<sup>3</sup>Institute of Surface-Earth System Science, Tianjin University, 92 Weijin Road, Nankai, Tianjin 300072, China*

*<sup>4</sup>School of Geography and Tourism, Qufu Normal University, Rizhao 276826, China*

*<sup>5</sup>Shandong Institute of Geological Sciences; Key Laboratory of Gold Mineralization Processes and Resource Utilization Subordinated to the Ministry of Land and Resources; Key Laboratory of Metallogenic Geological Process and Resources Utilization in Shandong Province, Jinan 250013, China*

*<sup>6</sup>Department of Earth Sciences, Natural History Museum, London SW7 5BD, UK*

*<sup>7</sup>State Key Laboratory of Biogeology and Environmental Geology, School of Earth Sciences and Resources, China University of Geosciences, Beijing 100083, China*

## **METHODS**

We measured Hg content at the Nanjing Institute of Geography and Limnology, Chinese Academy of Sciences (CAS), using the Hydra-C (LEEMAN LABS INC, America), a high-frequency atomic absorption spectrometer specifically designed for Hg determination with a lab determined detection limit of 0.5 ppb. Measurements are based on the direct thermal evaporation of Hg from solid samples and do not require chemical pretreatment of samples, thus avoiding potential contamination during sample preparation. Analyses were conducted on two aliquots. The accuracy was confirmed by the analysis of certified reference materials (GSS-27, Hg content of 116 ppb; GSD-10, Hg content of 280 ppb). Excellent correspondence to the certified values was obtained with a correlation coefficient of 0.99 and a standard residual deviation of 0.44. We re-analyzed 30 samples, especially including samples with Hg spikes, using the DMA-80 (Milestone, Italy) at the China University of Geosciences (Wuhan), and obtained similar results.

We measured Hg isotope ratios by coupling a customized cold vapor generation system to multi-collector inductively coupled plasma mass spectrometry (MC-ICPMS, Nu Plasma 3D) at Tianjin University using the methods of Huang et al. (2015) and Sun et al. (2020). Mass-dependent fractionation (MDF) of Hg isotopes is reported in  $\delta$  notation, which is the permil (‰) deviation relative to the NIST SRM 3133 standard. MIF of Hg isotopes is reported using the  $\Delta$  notation, which is the deviation of the measured isotope ratio from the theoretical ratio predicted by MDF. The mass discrimination effect is calibrated with Tl (Nist arm 997) standard solution. The analytical quality was controlled by repeated measurement of standard materials.

The long-term analysis gave average values of  $-0.04 \pm 0.1\%$  for  $\Delta^{199}\text{Hg}$  of UM-Almaden Hg (2SD, n=30). The 2SD of the isotopic compositions of the UM-Almaden were considered as the analytical uncertainty for the isotopic compositions of samples. When the uncertainty of the replicate isotopic measurements of one sample was larger than the 2SD of the UM-Almaden, the uncertainty was applied to the sample.

We conducted geochemical analyses of  $\delta^{13}\text{C}_{\text{org}}$  and total organic carbon (TOC) content, and  $\delta^{13}\text{C}_{\text{carb}}$  at the Nanjing Institute of Geology and Palaeontology, Chinese Academy of Sciences. Methods of analyses of  $\delta^{13}\text{C}_{\text{org}}$  and TOC are referred to Zhao et al. (2021). Methods of analyses of  $\delta^{13}\text{C}_{\text{carb}}$  are referred to Yu et al. (2018).

We conducted geochemical analyses of elements Al and S contents using an Agilent 710 Inductively coupled plasma-optical emission spectrometry (ICP-OES). The power of the RF generator for operating optimal parameters was 1200 W. Plasma gas flow, and auxiliary gas flow was 18 and 2.25 (L/min). The nebulizer gas pressure was 200 kPa. Sample reading time and initial stabilization time were 5 and 15 s, respectively. Injection delay time and rinse time were 40 and 15 s. The measurement replicate was three times. Type of detector Solid-state and spray chamber was CCD and Cyclonic, Modified Lichte, respectively. The sample delivery pump type was four-channel, software-controlled; peristaltic pump enables exact sample flows. We used fast pump mode and the pump speed was 15 rpm.

## **RESULTS**

The correlation of charophyte and ostracode biozones with the geomagnetic

polarity time scale was well established in China and Europe. Li et al. (2019) have established four charophyte biozones and one superzone and correlated it to the Geomagnetic Polarity Time Scale (GPTS) in the Songliao Basin. The latter three zones are grouped within the *Microchara cristata* Superzone, which allows intra- and intercontinental correlation with other basins in China and Europe, and the first appearance of *Peckichara sinuolata* lying in chron C29r was proposed as the basal marker of the Paleocene. Vicente et al. (2015) have established charophyte biozonation for the non-marine Maastrichtian–lowermost Paleocene deposits in the South-Eastern Pyrenean Vallcebre Basin and calibrated it to the GPTS. *P. varians* is a cosmopolitan species in freshwater lakes of the Eurasian Paleocene (Li et al., 2016), and its appearance is widely thought to represent the Paleocene in the Pingyi Basin. The *M. cristata* zone in the Pingyi Basin is an interval zone that started with the FAD of *M. cristata* and ended with the FAD of *P. varians*. Galbrun et al. (1993) have established five charophyte zones at Fontllonga, Àger Basin, northeast Spain, correlated with GPTS. The K/Pg boundary occurs in the uppermost part of the *Microchara cristata* subzone, which includes the Late Cretaceous and Early Palaeocene species. Riveline et al. (1996) have established 46 charophyte biozones for Mesozoic and Cenozoic charophyte biozonation correlated with GPTS and proposed the *Peckichara llobregatensis* zone as an early Danian biozone. Therefore, the correlation of charophytes and ostracodes biozones with the global nannofossils and planktonic foraminiferal biozones can be connected through GPTS (Fig. 1s).

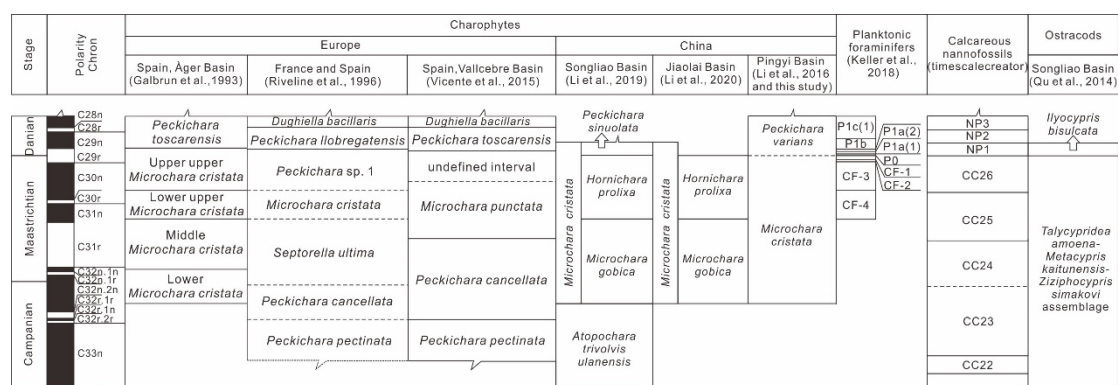


Figure 1s. Correlation of the Late Cretaceous–early Palaeocene charophyte (Galbrun et al., 1993; Riverline et al., 1996; Vicente et al., 2015; Li et al., 2016, 2019, 2020), planktonic foraminiferal, calcareous nannofossil and ostracod biozonation, calibrating with the GPTS. Planktonic foraminiferal zonation is cited from Keller et al. (2018). Calcareous nannofossil zones are generated from timescalecreator. Ostracod zones are cited from Qu et al. (2014).

In order to assess secular variation in Hg enrichment of the Pingyi Basin, mean Hg/TOC values were calculated for pre-Hg spike, Hg spike, and post-Hg spike intervals. The latter two intervals values are expressed as enrichment factors (EF) relative to pre-Hg spike interval values, where  $Hg-EF = (Hg/TOC)/(Hg/TOC)_{bg}$ , with ‘bg’ representing background (pre-Hg spikes) values. Mean Hg/TOC values for pre-Hg spike, Hg spike, and post-Hg spike intervals are 31.49, 520.62, and 25.48, respectively, calculated in Table 1 of supplementary information. The enrichment factors of Hg spike and post-Hg spike intervals are 16.54 and 0.81, respectively.

In order to assess secular variation in Hg enrichment of the Jiaolai Basin, mean Hg/Al values were calculated for pre-Hg spike, Hg spike, and post-Hg spike intervals. The latter two intervals values are expressed as EF relative to pre-Hg spike interval

values, where  $Hg-EF = (Hg/Al)/(Hg/Al)_{bg}$ , with 'bg' representing background (pre-Hg spikes) values. Mean Hg/Al values for pre-Hg spike, Hg spike, and post-Hg spike intervals are 5.7, 8.71, and 5.32, respectively, calculated in Table 1 of supplementary information. The enrichment factors of Hg spike, and post-Hg spike intervals are 1.53 and 0.93, respectively. Two figures (Figs. 2s, 3s) which focus on Hg spike-intervals in the Jiaolai and Pingyi basins were added.

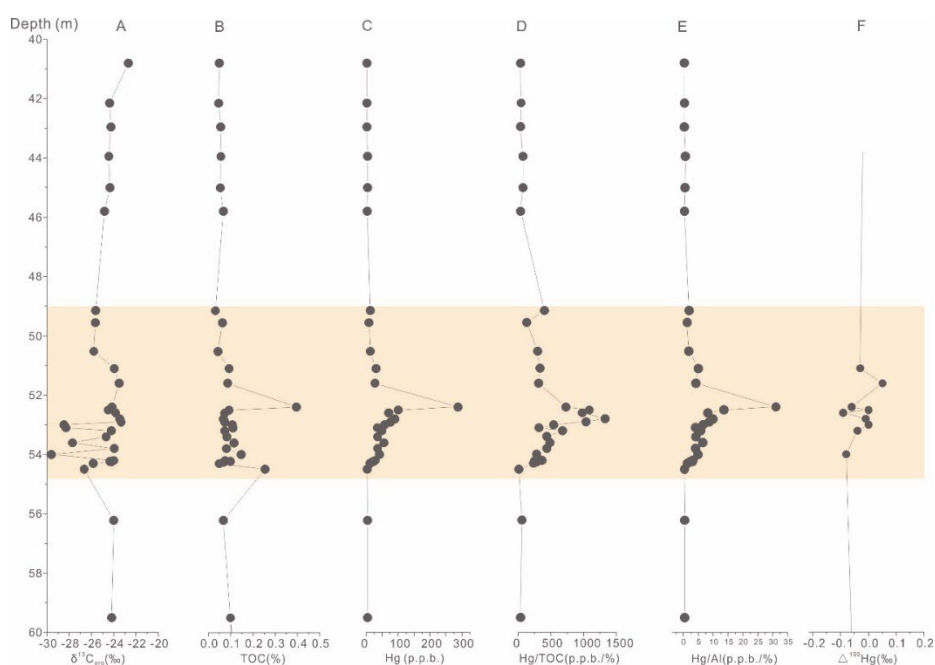


Figure 2s. Details focusing on the Hg spike interval in the Jiaolai Basin: (A)  $\delta^{13}C_{org}$ ; (B) TOC; (C) Hg; (D) Hg/TOC; (E) Hg/Al; and (F)  $\Delta^{199}Hg$ .

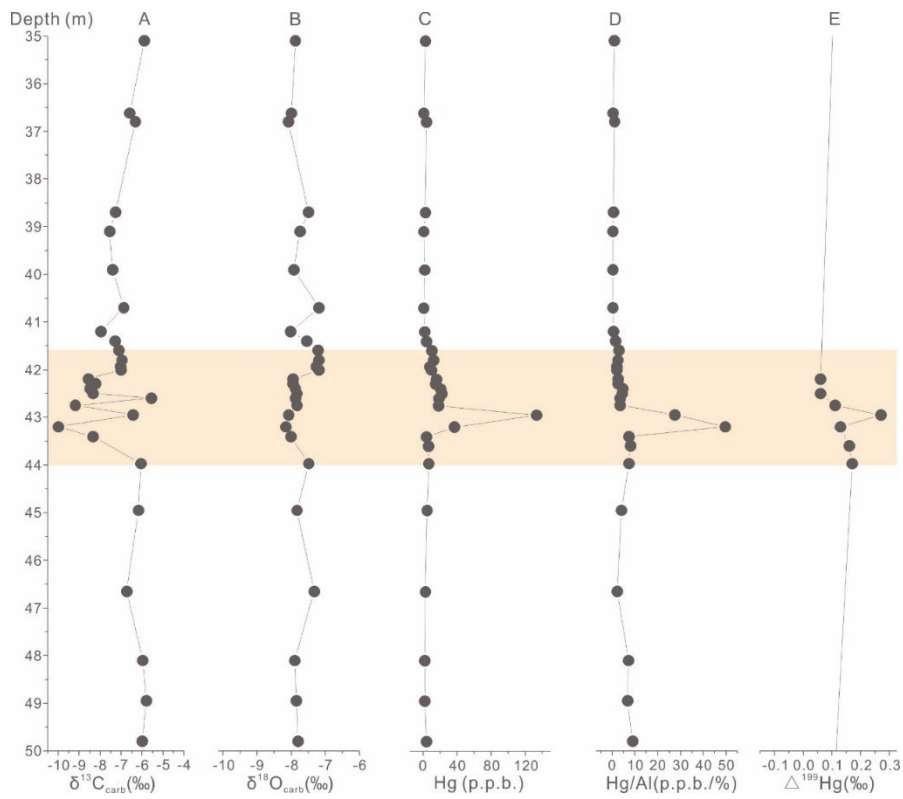


Figure 3s. Details of data focusing on Hg spike interval in the Pingyi Basin: (A)  $\delta^{13}\text{C}_{\text{org}}$ ; (B) TOC; (C) Hg; (D) Hg/TOC; and (E)  $\Delta^{199}\text{Hg}$ .

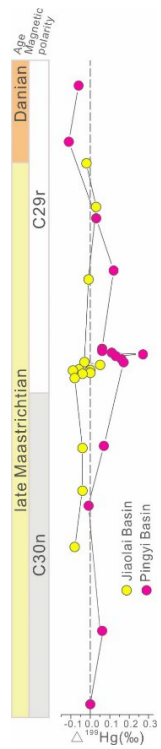


Figure 4s. Comparison of Hg MIF at the same horizontal scales for the two KPg sections in the

Jiaolai and Pingyi basins.

In the Jiaolai Basin, Hg concentrations are very low (mostly < 4 ppb), with peak Hg values, between 0–287 ppb, occurring at depths between 54.30–49.15 m (Fig. 2C in the main text). Aluminum (Al) ranges from 1.10 to 11.97% (mostly 5% to 10%), and total organic carbon (TOC) ranges from 0.032 to 0.395% (Fig. 2B in the main text), but remains above 0.2 % at the layer of Hg spikes (at a depth of 52.4 m). Where 0.2 % TOC marks the lowest level that Hg/TOC ratios can be reliably calculated (Grasby et al., 2019). Total sulfur (TS) ranges from 26 to 1179 ppb. Hg concentration shows no correlation with clay content (Hg and Al correlation analysis,  $r = -0.009$ ,  $n = 85$ ), and TS ( $r = -0.052$ ,  $n = 85$ ), but a correlation with TOC ( $r = 0.253$ ,  $p < 0.05$ ,  $n = 85$ ). In the Pingyi Basin, peak Hg values up to 133 ppb occur between 43.97 to 41.60 m in depth (Fig. 3C in the main text). Aluminum (Al) ranges from 0.14 to 8.25% (mostly 0.5 to 5%); and total organic carbon (TOC) ranges from 0.01 to 2.05% (Fig. 2B in main text). Total sulfur (TS) ranges from 133 to 13383 ppb. Hg contents show strong covariation with Al ( $r = 0.288$ ,  $p < 0.01$ ,  $n = 112$ ) and TOC ( $r = 0.258$ ,  $p < 0.01$ ,  $n = 111$ ), but not TS ( $r = 0.146$ ,  $n=112$ ), suggesting that TOC and Al are the dominant Hg hosts. However, TOC in the Pingyi Basin is quite low, mostly below 0.2 %, such that organic matter cannot have had a strong influence on Hg sequestration, so Al was used for Hg normalization instead (Fig. 3D in the main text).

Correlation with other existing terrestrial and marine Hg records and existing carbon isotope records (Sial et al., 2013; Sial et al., 2014; Font et al., 2016; Sial et al.,

2016; Percival et al., 2018; Fendley et al., 2019; Keller et al., 2020; Gilabert et al., 2021) was conducted (Figs. 5s, 6s).

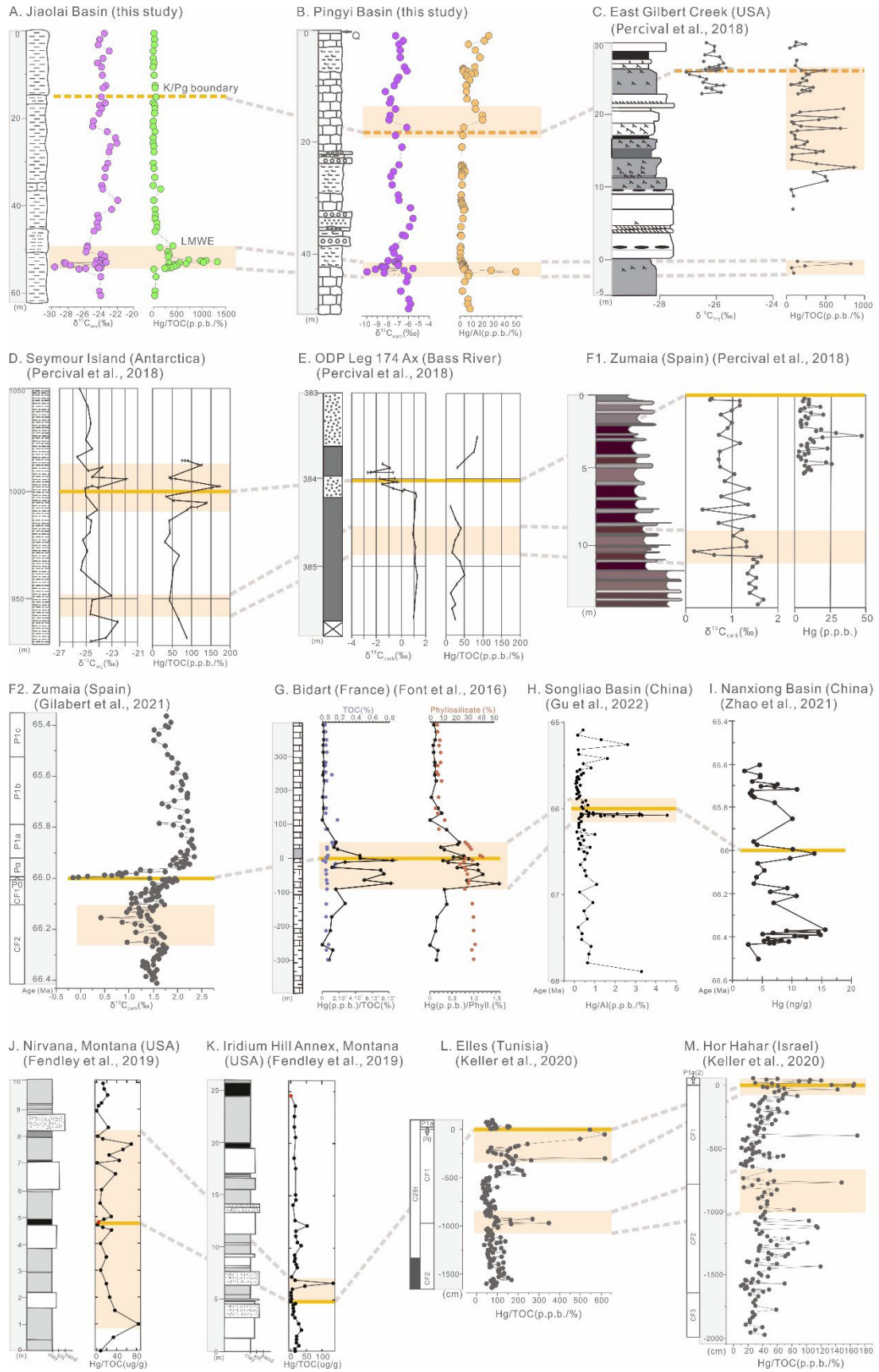


Figure 5s. Comparison of Hg/TOC from East Gilbert Creek (USA), Seymour Island (Antarctica), ODP Leg 174 Ax (Bass River), Bidart (France), Nirvana, Montana (USA), Iridium Hill Annex, Montana (USA), Elles (Tunisia), and Hg data from Zumaia (Spain), the Nanxiong Basin (China), and Hor Hahar (Israel) (where TOC contents were below error or not available), and Hg/Al data from the Songliao Basin (China). Comparison of  $\delta^{13}\text{C}_{\text{org}}$  from East Gilbert Creek (USA), Seymour Island (Antarctica), and  $\delta^{13}\text{C}_{\text{carb}}$  from ODP Leg 174 Ax (Bass River), Zumaia (Spain), and Elles (Tunisia).

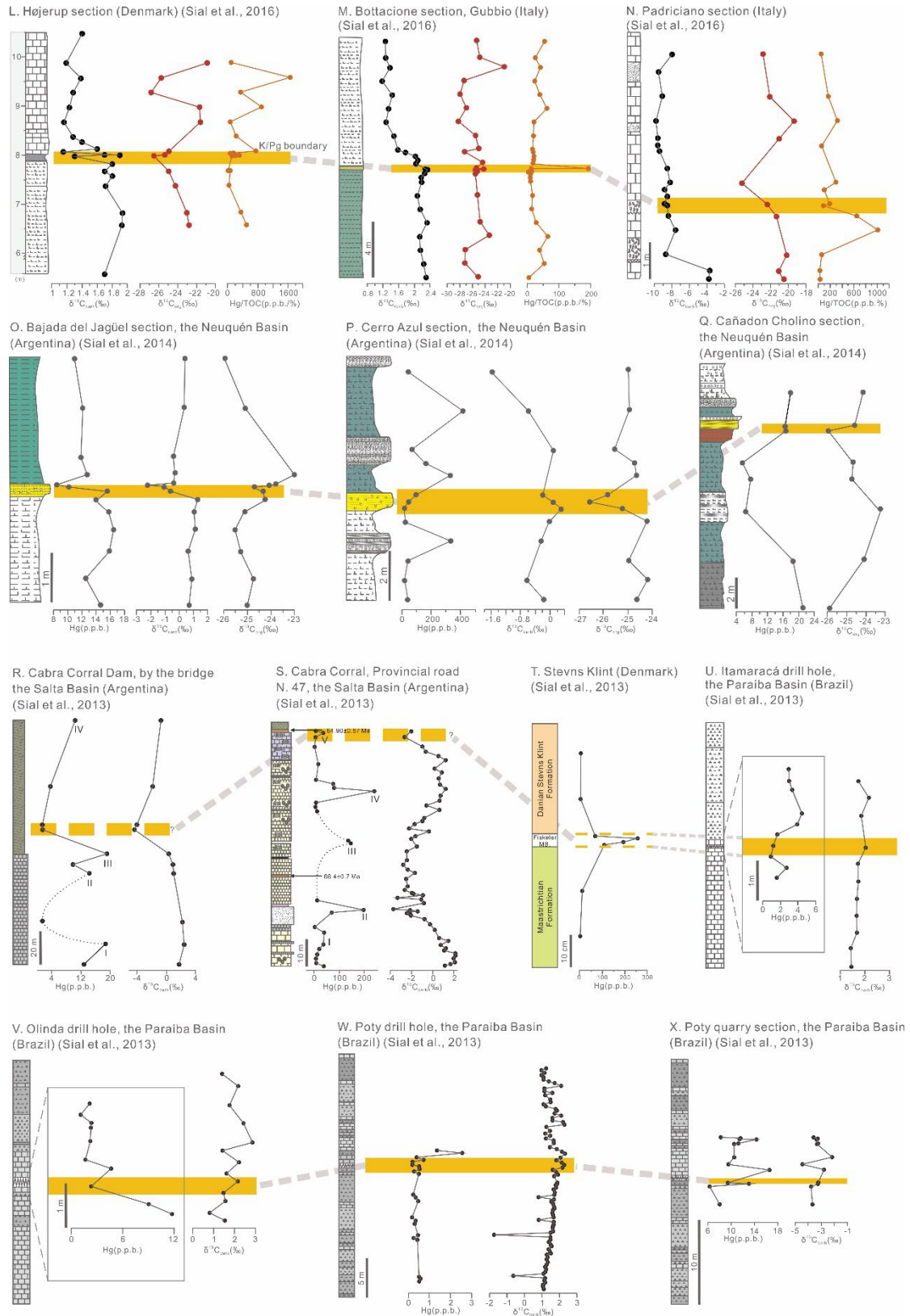


Figure 6s. Comparison of Hg/TOC from Højerup section (Denmark), Bottacione section, Gubbio (Italy), Padriciano section (Italy), and Hg data from Bajada del Jagüel section, the Neuquén Basin (Argentina), Cerro Azul section, the Neuquén Basin (Argentina), Cañadon Cholino section, the

Neuquén Basin (Argentina), Cabra Corral Dam, by the bridge the Salta Basin (Argentina), Cabra Corral, Provincial road N. 47, the Salta Basin (Argentina), Stevns Klint (Denmark), Itamaracá drill hole, the Paraíba Basin (Brazil), Olinda drill hole, the Paraíba Basin (Brazil), Poty drill hole, the Paraíba Basin (Brazil), and Poty quarry section, the Paraíba Basin (Brazil) (where TOC contents were below error or not available). Comparison of  $\delta^{13}\text{C}_{\text{org}}$  and  $\delta^{13}\text{C}_{\text{carb}}$  from Højerup section (Denmark), Bottaccione section, Gubbio (Italy), Padriciano section (Italy), Bajada del Jagüel section, the Neuquén Basin (Argentina), Cerro Azul section, the Neuquén Basin (Argentina); comparison of  $\delta^{13}\text{C}_{\text{org}}$  from the Cañadon Cholino section, the Neuquén Basin (Argentina); comparison of  $\delta^{13}\text{C}_{\text{carb}}$  from Cabra Corral Dam, by the bridge, the Salta Basin (Argentina), Cabra Corral, Provincial road N. 47, the Salta Basin (Argentina), Itamaracá drill hole, the Paraíba Basin (Brazil), Olinda drill hole, the Paraíba Basin (Brazil), Poty drill hole, the Paraíba Basin (Brazil), and Poty quarry section, the Paraíba Basin (Brazil).

Micropaleontological studies were conducted and charophyte and ostracod species are listed in Table 2 of supplementary information. Our paleontological data indicate the first appearances of charophytes *Sphaeorchara jacobii* and *Lychnothamnus* aff. *vectensis* in the Pinyi Basin and the first appearance of *L.* aff. *vectensis* in the Jiaolai Basin during the Hg spike interval, indicating increasing charophyte range-through diversity (a species is considered present in a sample if found both below and above). *Cypridea* (*Cypridea*) *pingyiensis* first appeared during the Hg spike interval in the Pingyi Basin, revealing increasing ostracod range-through diversity.

## REFERENCES CITED

- Fendley, I. M., Mittal, T., Sprain, C. J., Marvin-DiPasquale, M., Tobin, T. S., and Renne, P. R., 2019, Constraints on the volume and rate of Deccan Traps flood basalt eruptions using a combination of high-resolution terrestrial mercury records and geochemical box models: *Earth and Planetary Science Letters*, v. 524, 115721, <https://doi.org/10.1016/j.epsl.2019.115721>.
- Font, E., Adatte, T., Sial, A. N., Drude de Lacerda, L., Keller, G., and Punekar, J., 2016, Mercury anomaly, Deccan volcanism, and the end-Cretaceous mass extinction: *Geology*, v. 44, no. 2, p. 171–174, <https://doi.org/10.1130/g37451.1>.
- Galbrun, B., Feist, M., Colombo, F., Rocchia, R., and Tambareau, Y., 1993, Magnetostratigraphy and biostratigraphy of Cretaceous–Tertiary continental deposits, Ager basin, province of Lerida, Spain: *Palaeogeography, Palaeoclimatology, Palaeoecology*, v. 102, no. 1, p. 41–52, [https://doi.org/10.1016/0031-0182\(93\)90004-3](https://doi.org/10.1016/0031-0182(93)90004-3).
- Gilbert, V., Batenburg, S. J., Arenillas, I., and Arz, J. A., 2021, Contribution of orbital forcing and Deccan volcanism to global climatic and biotic changes across the Cretaceous-Paleogene boundary at Zumaia, Spain: *Geology*, v. 50, no.1, p. 21–25, <https://doi.org/10.1130/g49214.1>.
- Grasby, S. E., Them, T. R., Chen, Z., Yin, R., and Ardakani, O. H., 2019, Mercury as a proxy for volcanic emissions in the geologic record: *Earth-Science Reviews*, v. 196, 102880, <https://doi.org/10.1016/j.earscirev.2019.102880>.
- Huang, Q., Liu, Y., Chen, J., Feng, X., Huang, W., Yuan, S., Cai, H., and Fu, X., 2015, An improved dual-stage protocol to pre-concentrate mercury from airborne particles for precise isotopic measurement: *Journal of Analytical Atomic Spectrometry*, v. 30, no. 4, p. 957–966, <https://doi.org/10.1039/C4JA00438H>.
- Keller, G., Mateo, P., Monkenbusch, J., Thibault, N., Punekar, J., Spangenberg, J. E., Abramovich, S., Ashkenazi-Polivoda, S., Schoene, B., Eddy, M. P., Samperton, K. M., Khadri, S. F. R., and Adatte, T., 2020, Mercury linked to Deccan Traps volcanism, climate change and the end-Cretaceous mass extinction: *Global and Planetary Change*, v. 194, 103312, <https://doi.org/10.1016/j.gloplacha.2020.103312>.
- Keller, G., Mateo, P., Punekar, J., Khozyem, H., Gertsch, B., Spangenberg, J., Bitchong, A. M., and Adatte, T., 2018, Environmental changes during the Cretaceous-Paleogene mass extinction and Paleocene-Eocene Thermal Maximum: implications for the Anthropocene: *Gondwana Research*, v. 56, p. 69–89, <https://doi.org/10.1016/j.gr.2017.12.002>.
- Li, S., Wang, Q. F., Zhang, H. C., Lu, H. N., and Martín-Closas, C., 2016, Charophytes from the Cretaceous–Paleogene transition in the Pingyi Basin (eastern China) and their Eurasian correlation: *Cretaceous Research*, v. 59, p. 179–200, <https://doi.org/10.1016/j.cretres.2015.10.022>.
- Li, S., Wang, Q. F., Zhang, H. C., Wan, X. Q., and Martín-Closas, C., 2019, Charophytes from the Cretaceous–Paleocene boundary in the Songliao Basin (north-eastern China): a Chinese biozonation and its calibration to the Geomagnetic Polarity Time Scale: *Papers in Palaeontology*, v. 5, no. 1, p. 47–81, <https://doi.org/10.1002/spp2.1225>.
- Li, S., Wang, Q. F., Zhang, H. C., Wang, H., and Wan, X. Q., 2020, Latest Campanian to Maastrichtian charophytes in the Jiaolai Basin (eastern China): *Cretaceous Research*, v. 106, 104266,

- <https://doi.org/10.1016/j.cretres.2019.104266>.
- Percival, L. M. E., Jenkyns, H. C., Mather, T. A., Dickson, A. J., Batenburg, S. J., Ruhl, M., Hesselbo, S. P., Barclay, R., Jarvis, I., Robinson, S. A., and Woelders, L., 2018, Does large igneous province volcanism always perturb the mercury cycle? Comparing the records of Oceanic Anoxic Event 2 and the end-Cretaceous to other Mesozoic events: *American Journal of Science*, v. 318, no. 8, 799, <https://doi.org/10.2475/08.2018.01>.
- Qu, H. Y., Xi, D. P., Li, S., Paul, C. J., Huang, Q. H., and Wan, X. Q., 2014, Late Cretaceous-early Paleocene ostracod biostratigraphy of Scientific Drilling Sk1 (N) in the Songliao Basin, northeast China: *Journal of Paleontology*, v. 88, no. 4, p. 786–798, <https://doi.org/10.1666/13-076>.
- Riveline, J., Berger, J. P., Feist, M., Martín-Closas, C., Schudack, M., and Soulié-Märsche, I., 1996, European Mesozoic-Cenozoic charophyte biozonation: *Bulletin de la Société géologique de France*, v. 167, no. 3, p. 453–468, <https://pubs.geoscienceworld.org/sgf/bsgf/article/167/3/453/122848/European-Mesozoic-Cenozoic-charophyte-biozonation>.
- Sial, A. N., Chen, J., Lacerda, L. D., Frei, R., Tewari, V. C., Pandit, M. K., Gaucher, C., Ferreira, V. P., Cirilli, S., Peralta, S., Korte, C., Barbosa, J. A., and Pereira, N. S., 2016, Mercury enrichment and Hg isotopes in Cretaceous–Paleogene boundary successions: links to volcanism and palaeoenvironmental impacts: *Cretaceous Research*, v. 66, p. 60–81, <https://doi.org/10.1016/j.cretres.2016.05.006>.
- Sial, A. N., Chen, J., Lacerda, L. D., Peralta, S., Gaucher, C., Frei, R., Cirilli, S., Ferreira, V. P., Marquillas, R. A., Barbosa, J. A., Pereira, N. S., and Belmino, I. K. C., 2014, High-resolution Hg chemostratigraphy: a contribution to the distinction of chemical fingerprints of the Deccan volcanism and Cretaceous–Paleogene Boundary impact event: *Palaeogeography, Palaeoclimatology, Palaeoecology*, v. 414, p. 98–115, <https://doi.org/10.1016/j.palaeo.2014.08.013>.
- Sial, A. N., Lacerda, L. D., Ferreira, V. P., Frei, R., Marquillas, R. A., Barbosa, J. A., Gaucher, C., Windmüller, C. C., and Pereira, N. S., 2013, Mercury as a proxy for volcanic activity during extreme environmental turnover: the Cretaceous–Paleogene transition: *Palaeogeography, Palaeoclimatology, Palaeoecology*, v. 387, p. 153–164, <https://doi.org/10.1016/j.palaeo.2013.07.019>.
- Sun, R., Yuan, J., Sonke, J. E., Zhang, Y., Zhang, T., Zheng, W., Chen, S., Meng, M., Chen, J., Liu, Y., Peng, X., and Liu, C., 2020, Methylmercury produced in upper oceans accumulates in deep Mariana Trench fauna: *Nature Communications*, v. 11, no. 1, 3389, <https://doi.org/10.1038/s41467-020-17045-3>.
- Tian, J.-X., Chen, J., Lu, H.-N., Chen, C., Wang, H., Li, T., Li, S., Wang, Q.-F., Zhang, H.-C., and Wan, X.-Q., 2021, Discovery of charophyte flora across the Cretaceous–Paleocene transition in the Jiaolai Basin: *Palaeoworld*, v. 30, no. 3, p. 538–550, <https://doi.org/10.1016/j.palwor.2020.09.007>.
- Vicente, A., Martín-Closas, C., Arz, J. A., and Oms, O., 2015, Maastrichtian–basal Paleocene charophyte biozonation and its calibration to the Global Polarity Time Scale in the Southern Pyrenees (Catalonia, Spain): *Cretaceous Research*, v. 52, p. 268–285, <https://doi.org/10.1016/j.cretres.2014.10.004>.
- Yu, Z., Wang, X., Han, G., Liu, X., and Zhang, E., 2018, Organic and inorganic carbon and their stable

isotopes in surface sediments of the Yellow River Estuary: *Scientific Reports*, v. 8, no. 1, p. 10825, <https://doi.org/10.1038/s41598-018-29200-4>.

Zhao, X., Wang, W., Xie, G., Pan, S., Jarzembowski, E. A., and Zheng, D., 2021, Depositional environment of Middle Triassic organic-rich shales in the Ordos Basin, northwest China: *Geological Journal*, v. 56, no. 9, p. 4849–4860, <https://doi.org/10.1002/gj.4215>.